Article

Study on the Formation Mechanism of Cold-Rolled Sludge and the Biodiesel Production from Sludge

Mengke Zhou, Peng Jiang, Yichao Hu, Muhammad-Faryad Ali, and Xiaolong Zhou*

Read Online

ACCESS | Metrics & More | Article Recommendations

ABSTRACT: Cold-rolled sludge (CRS) has become a challenge due to its large volumetric capacity and high toxicity and is difficult to be degraded under natural conditions. This article aims to explore the feasibility of the solvent extraction method for recovering oil and fat from CRS and utilizing it as a raw material to prepare biodiesel with the application of a homogeneous catalyst H_2SO_4 to mediate esterification and transesterification. The formation mechanism of CRS was proposed with its detailed analysis; hydroxylates were preferentially adsorbed on the metal surface by hydrogen bonds, and free fatty acids were hooked by carbon chains to form a second layer of adsorption. It revealed the reason for the residual oil content on the surface of the extracted solid phase. Experimental data represented an optimum biodiesel yield of 96.5% at a catalyst dosage of 25 wt %, a reaction time of 24 h, a methanol-to-oil molar ratio of 70:1, and a reaction temperature of 60 °C. The main properties of the biodiesel were tested and confirmed to meet ASTM D6751 standards.
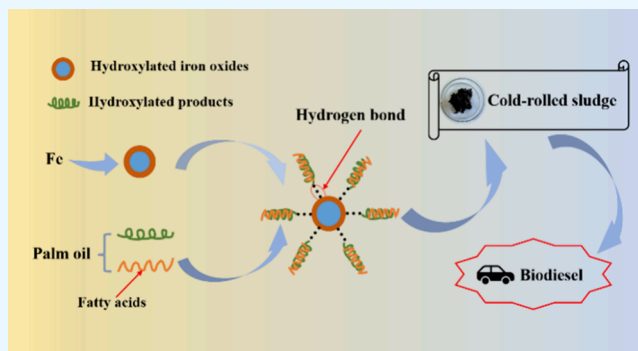
1. INTRODUCTION

Cold-rolled sludge (CRS), as an inevitable byproduct of steel production, has attracted the attention of researchers because of its large volume and strong potential to deliver valuable components after effective treatment.[1] The traditional CRS treatment can be divided into harmless disposal and resource utilization technologies. Solidification and incineration are common methods of its harmless disposal,[2,3] having the advantages of simple operation and easy handling, but various toxic intermediates are produced during the process, resulting in a massive damage to the human body and environment.[4] On the other hand, resource utilization technologies aimed at reusing iron or oil including pyrolysis,[5] freeze−thaw,[6] ultrasonic-microwave treatment,[7] and solvent extraction, offer sustainable approaches to the treatment of CRS and align with principles of resource conservation.

Solvent extraction is a simple solution for the simultaneous recovery of both micronized iron powder and oil. Chen et al.[8] extracted iron, nickel, and chromium from stainless sewage sludge utilizing solvent extraction; the results showed that the extraction efficiencies of iron, nickel, and chromium were respectively 97.6, 98.1, and 95.7%. Yaseen et al.[9] extracted 91 wt % of hydrocarbons from spent engine oil by a blend of 10% ethyl acetate with *n*-hexane as eluent. In addition, Zhao et al.[10] found that ethylene dichloride had more excellent ability in dissolving cold rolling oil; it can effectively recover waste oil. Solvent extraction has been extensively studied in the field of recovering waste oil. The form of oil solids present in the CRS

is a crucial factor affecting solvent extraction, so the selection of a suitable solvent mixture is essential for the extraction of the oil.

Utilizing extracted oil to produce biodiesel provides a new idea for the resourceful use of CRS. Biodiesel, as a sustainable biomass fuel, has the advantages of biodegradability, nontoxicity, low sulfur content, high cetane number, and high flash point.[11] Despite the wide feedstocks of biodiesel, the cost of raw materials takes up as much as 70−80% of the total cost. Therefore, utilizing the extracted oil to prepare biodiesel not only addresses the challenge of treating CRS but also seeks a cost-effective alternative source of oil for the preparation of biodiesel.[12] In addition, acidic catalysts are not limited by raw materials, especially H_2SO_4, which has an excellent performance in preparing biodiesel from high acid-value oil.[13,14]

In this study, the formation mechanism of CRS was innovatively proposed via different analyses. In addition, a mixture of 1,2-dichloroethylene/isopropyl alcohol was used to extract the oil from the CRS sample along with Box-Behnken Design response experiments to evaluate the effects of the

solvent-to-oil mass ratio, extraction time, and extraction temperature on the extraction efficiency. Meanwhile, biodiesel was prepared using extracted oil from CRS, and the effects of the dosage of the catalyst, the molar ratio of alcohol to oil, reaction time, and reaction temperature on the biodiesel yield were also investigated. The feasibility of preparing biodiesel from CRS has been verified for the first time, expanding a new perspective for the source of biodiesel raw materials.

2. MATERIALS AND METHODS

2.1. Chemicals. The CRS sample used in this study was provided by the Jiangsu Xiehe steel rolling factory in China. Reagents including 1,2-dichloroethane (AR), toluene (AR), methanol (AR), isopropyl alcohol (AR), hexane (AR), sulfuric acid (98 wt %), potassium hydroxide (85.0 wt %), sodium chloride (99.5 wt %), palm oil methyl ester (99 wt %), linoleic acid methyl ester (95 wt %), stearic acid methyl ester (99 wt %), oleic acid methyl ester (99 wt %), and cinnamic acid methyl ester (98 wt %) were all purchased from Shanghai Titan Co., Ltd., China. All solutions were prepared with deionized water.

2.2. Experimental Setup and Procedure. *2.2.1. Oil Extraction from CRS.* All experiments were carried out in a 500 mL three-necked flask equipped with a mechanical agitator (EUROSTAR IKA-WERKE, China) and a condenser tube, as shown in Figure 1. First, 50 g of CRS sample was mixed with
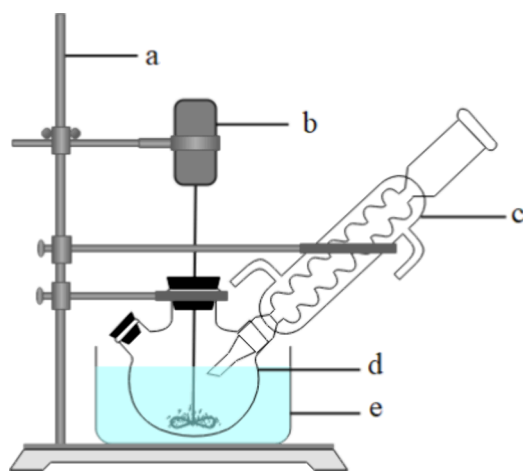
Figure 1. Experimental setup: (a) iron stand, (b) mechanical agitator, (c) condenser distillation column, (d) three-necked flask, and (e) oil bath.

250 g of mixed solvents (the mass ratio of 1.2-dichloroethane to isopropyl alcohol of 6:1) and then added into the flask. The flask was sealed with a sealing film, and the mixture was mechanically stirred to 300 rpm at 80 °C for 4 h. Subsequently, the organic phase and solid phase were separated by centrifugation at 10000 rpm for 15 min using a high-speed centrifuge (XIANGYI 1080, China). Finally, the solvent in the organic phase was recovered by distillation through the device shown in Figure 2. The methylated products were analyzed by gas chromatography−mass spectrometry (GC-MS) to determine the composition of the extracted oil.

2.2.2. Biodiesel Preparation. Thirty grams of extracted oil was poured into the three-necked flask along with methanol injected into it (the molar ratio of methanol to oil is 70:1). Concentrated sulfuric acid (25 wt % of extracted oil) was
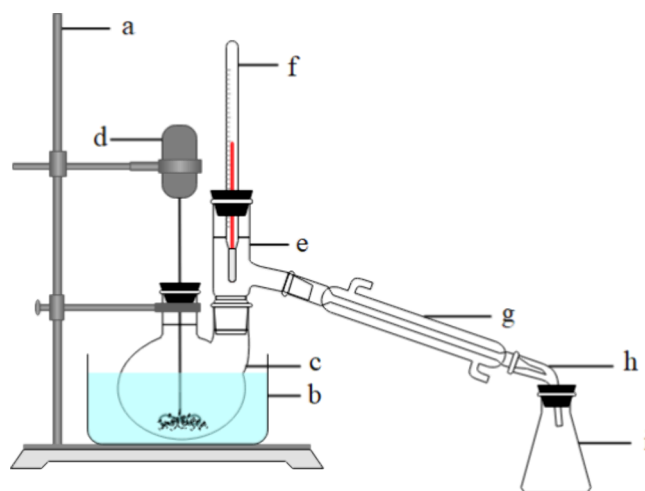
Figure 2. Condensate reflux device: (a) iron stand, (b) oil bath, (c) flask, (d) mechanical agitator, (e) tube with two joints, (f) thermometer, (g) condenser distillation column, (h) vacuum connecting tube, and (i) conical flask.

selected as a homogeneous catalyst for the biodiesel preparation, while it was diluted with methanol (0.1 g/g) to avoid direct oxidation of the extracted oil. Subsequently, the flask was sealed using a rubber stopper, and the speed of stirring was set to 300 rpm at 60 °C for 24 h. After the reaction was completed, excess methanol was removed by evaporation, and the product was transferred in the apparatus shown in Figure 2. The biodiesel remaining at the bottom of the flask was treated according to a classical procedure.[15] First, the biodiesel was dissolved in *n*-hexane, and then the mixture was transferred to a separatory funnel, followed by repeated washing with warm deionized water to remove H_2SO_4 and glycerol. Subsequently, the organic phase after being washed was heated at 80 °C until the weight remained constant to remove *n*-hexane. The yield of biodiesel in the product was analyzed by GC-MS.

2.3. Analysis Methods. *2.3.1. Analysis of the Sludge Sample.* The oil content of the sludge sample was analyzed by extraction with toluene according to US EPA3540C-1196.[16] The water content was measured by a drying operation based on ASTM D95-18, and the solid content was calculated by eq 1:[17]

$$\text{solid\%} = 100\% - \text{oil\%} - \text{water\%} \tag{1}$$

The saponification value and acid value were measured using acid−alkali neutralization titration in different systems, which was in line with ASTM D974-21.[18] Density was tested by the pycnometer method according to ASTM D891-18.[19]

2.3.2. Analysis of Extracted Oil. The composition of the extracted oil was identified using a GC-MS system (Agilent 7890B, US) after catalytic derivatization by sodium methoxide.[20] The GC-MS system was equipped with an HP-5 capillary column (30 m × 0.25 mm × 0.25 μm), and the applied temperature was programmed as follows: from 30 to 150 °C at 3 °C/min for 2 min, followed by 280 °C at 5 °C/min for 25 min. The carrier gas was high-purity nitrogen at a flow rate of 1.5 mL/min. A 5 mL volume of the headspace volume was taken into the syringe and injected into the GC system with a splitting ratio of 10:1 without delay. The mass analysis was performed under 70 eV electron impact ionization mode with an MS scan from 35 to 450 *m/z*. The ion source

and quadrupole temperatures were 230 and 150 °C, respectively.

2.3.3. Analysis of Extracted Solid. The functional groups of extracted solid were identified using Fourier transform infrared spectroscopy (FT-IR, Nicolet 6700, USA).[21] X-ray photoelectron spectroscopy (XPS, Thermo Scientific K-Alpha, UK) was used to measure the electron energy distribution and the relative strength of electrons at different energies of the extracted solid.[22] Microscopic morphology was observed by scanning electron microscopy (SEM, FEI-SEM, USA) with a TVIPS F416 camera.[23]

The residual oil content of the extracted solid was determined by calcination in a muffle furnace (KF1200, China) at 800 °C with a heating rate of 3 °C/min for 3 h. The extracted solid residual oil content (SR, %) was calculated by eq 2:

$$SR\% = \frac{M_0 - \frac{112}{160}M_1}{M_0} \times 100\% \tag{2}$$

where M_0 and M_1 are the weights of the solid before and after calcination, respectively (g); 160 is the molar mass of Fe_2O_3, and 112 is the total molar mass of Fe in Fe_2O_3.

The organic matter on the surface of the extracted solid can be removed after calcination in a muffle furnace. Meanwhile, the metal elements in the calcined solid were oxidized, but their composition was not affected. Hence, the metal composition of the sludge can be obtained through the analysis of the calcined solid using sequential X-ray fluorescence spectroscopy (XRF, Shimadzu Corporation 1800, JPN).[24]

2.3.4. Analysis of Biodiesel. The biodiesel products were measured by GC-MS according to the experimental procedure described in Section 2.4, while *n*-hexane was selected as the solvent and methyl cinnamate was applied as the internal standard substance. The biodiesel yield and the mass of FAMEs were calculated by the following eqs 3 and 4:[25]

$$\text{biodiesel yield}\% = \frac{\text{weight of FAMEs in product}}{\text{weight of extracted oil from CRS}} \cdot 100\% \tag{3}$$

$$\text{weight of FAMEs} = \frac{\sum f_i A_i \cdot m_k}{A_k} \tag{4}$$

where A_i and A_k are the peak areas of the biodiesel produced and methyl cinnamate, respectively, m_k is the mass of methyl cinnamate, and f_i is the correction factor for fatty acids (palmitic acid, 1.1455; stearic acid, 1.2020; linoleic acid, 1.4498; oleic acid, 1.2230).

2.4. Response Surface Methodology. Most of the oil should be recovered from the sludge through solvent extraction, which can be assessed by the residual oil content in the extracted solid. Box-Behnken design (BBD) was employed to investigate the effect of operational variables on the residual oil content when a mixture of 1,2-dichloroethane/ isopropyl alcohol was used as the extraction solvent.

The experimental variables and levels were determined based on the results of previous single-factor extraction experiments, and the details are listed in Table 1. Meanwhile, the experimental conditions, the obtained residual oil content, and the four experiments replicated at the center point are demonstrated in Table 2.

Table 1. Experimental Range and Levels of the Variables

factor	unit	symbol	range and levels		
			low	middle	high
solvents-to-sludge ratio	g:g	X_1	4:1	5:1	6:1
extraction temperature	°C	X_2	70	80	90
extraction time	h	X_3	3	4	5

Table 2. Experimental design of the three independent variables and the results

order	manipulated variables			response, SR (%)
	X_1	X_2	X_3	
1	4:1	80	5	31.1
2	5:1	90	5	25.6
3	5:1	80	4	22.6
4	4:1	90	4	28.4
5	5:1	70	5	29.8
6	4:1	70	4	30.7
7	5:1	80	4	22.4
8	6:1	80	3	26.2
9	5:1	80	4	22.2
10	5:1	90	3	26.9
11	6:1	90	4	26.3
12	6:1	80	5	26.4
13	6:1	70	4	27.1
14	5:1	70	3	26.1
15	4:1	80	3	26.5
16	5:1	80	4	22.6
17	5:1	80	4	21.9

In addition, the effect of the three independent variables was investigated using the surface response method, which was analyzed through the software of Design Expert 8.0.6. The statistical significance of the model and identifying statistical terms were determined at a confidence level of 95%. The rationality of quadratic mathematical equations with data fitting was tested by the coefficient of determination (R^2) and its adjusted form (R^2_{adj}).

Meanwhile, the interaction of these three factors on the extraction results and the predicted response variable were also studied,[26] and the established model of a quadratic mathematical equation is shown in eq 5:

$$SR\% = \beta_0 + \sum_{i=1}^{3} \beta_i X_i + \sum_{i=1}^{3} \beta_{ii} X_i^2 + \sum_{i=1}^{3} \sum_{j>i}^{3} \beta_{ij} X_{ij} \tag{5}$$

where X_i and X_{ij} are the independent variables, and β_0 is a constant, while β_i, β_{ii}, and β_{ij} are linear, interaction, and quadratic parameters, respectively.

2.5. Quality Assurance of the Data. All procedures were repeated three times to ensure the reproducibility and reliability of the experimental results. The data presented have a standard deviation (SD) of less than 2%. The values in all graphs are the average values.

3. RESULTS AND DISCUSSION

3.1. Composition and Property of CRS and Extracted Oil and Solid. *3.1.1. Composition of CRS.* The characteristics of the CRS are listed in Table 3. The total amount of esters and free fatty acids in the sample can be assessed by the saponification value, which was determined to be 187.02 mg KOH/g. Simultaneously, the acid value of the CRS was 103.05

Table 3. Characteristics of the CRS

property	value	property	value
oil content (wt %)	62.80	saponification value (mg KOH/g)	187.02
water content (wt %)	21.65	acid value (mg KOH/g)	103.05
solid content (wt %)	15.55	density (g/mL)	0.71

mg KOH/g, which was significantly different from the value of fresh lubricating oil (9.5 mg KOH/g). The formation of large amounts of fatty acids originated from the severe hydrolysis of palm oil after prolonged usage.[27] The contents of oil, water, and solids of the CRS were determined as 62.80, 21.65, and 15.55%, respectively, indicating that oil was the main component of the CRS and had a high recycling value.

3.1.2. GC-MS Analysis. The composition of the oil in the sludge (Figure 3a) and extracted oil (Figure 3b) after being treated with methyl-esterification was analyzed by GC-MS. Also, the methylated products of CRS and extracted oil are shown in Table 4.
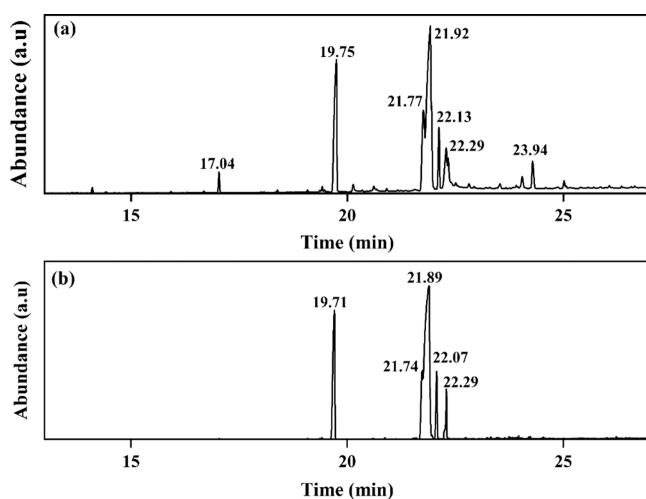
Figure 3. GC-MS spectrum of methylated products: (a) CRS; (b) extracted oil.

Table 4. Methylated Products of CRS Obtained from GC-MS

material	molecular formula	time	
		CRS	extracted oil
methyl myristate	$C_{15}H_{30}O_2$	17.04	
methyl palmitate	$C_{17}H_{34}O_2$	19.75	19.71
methyl 6,9-octadecadienoate	$C_{19}H_{34}O_2$	21.77	21.74
methyl 10-octadecenoate	$C_{19}H_{36}O_2$	21.92	21.89
methyl stearate	$C_{19}H_{38}O_2$	22.13	22.07
methyl 12-octadecenoate	$C_{19}H_{36}O_2$	22.29	22.29
methyl 9-hydroxy-octadecanoic	$C_{19}H_{36}O_3$	23.94	

As shown in Figure 3a, the main components of the methylated products were detected as methyl myristate (C14:0; 1.43%), methyl palmitate (C16:0; 21.46%), methyl stearate (C18:0; 4.73%), methyl oleate (C18:1; 49.50%), methyl linoleic acid (C18:2; 12.33%), and other acid methyl esters (10.55%). As can be observed, only several fatty acid methyl esters were detected without characteristic peaks about alkyl hydrocarbon, indicating the absence of mineral oil in the sludge, and the composition was similar to that of palm oil methyl ester.[28] Meanwhile, Figure 3b shows that extracted oil methylation products including methyl palmitate (C16:0; 20.67%), methyl stearate (C18:0; 6.52%), methyl oleate (C18:1; 62.44%), and methyl linoleic acid (C18:2; 10.37%). Compared to the cold-rolled sludge methylation product, the extracted oil methylation product contains more methyl stearate (+1.79%) and methyl oleate (+12.94%), less methyl palmitate (−0.79%) and methyl linoleic acid (−1.96%), and no other methylation products, which means that the purity of the extracted oil was improved, mainly composed of used palm oil.

3.1.3. XRF Analysis. Since sludge is a mixture of solids and organic matter, the samples cannot be directly tested for determination of the elemental composition of the solids. Consequently, the sludge was first calcined at a high temperature to remove the organic matter, and the remaining solids were taken to analyze their composition by an XRF measurement. As listed in Table 5, the most abundant metal

Table 5. Element Composition of the Solids in CRS

element	content (%)	element	content (%)
Fe	89.83	Si	0.11
O	8.75	Ni	0.09
Mn	0.23	Ca	0.08
As	0.19	Ti	0.08
Al	0.15	Mo	0.05
Zn	0.15	Pb	0.02
Cr	0.13	Nb	0.02
Cu	0.11	Zr	0.01

element in the calcined solid was determined to be iron with a content of 89.83%. This is consistent with the previous literature[10] reporting that iron is the dominant element in the solid of CRS.

3.2. The Formation Mechanism of CRS. The formation mechanism of cold-rolled sludge is one of the focuses of this study and has rarely been mentioned in the previous literature. The formation of oil sludge was a slow process in which organic matter adsorbed on the surface of iron powder gradually increased. Thus, iron powders with different residual oil contents were analyzed, which were obtained by different rounds of extraction of the CRS sample.

3.2.1. SEM Analysis. The microscopic morphology of the recovered solids after extraction was investigated by a SEM analysis. According to SEM images in Figure 4a, numerous lumpy and flaky structures were distributed on the surface of the solids recovered after single extraction, indicating that there was a large amount of organic matter adhering to the surface of the iron powders, which was also verified by the analysis of elemental distribution on the surface based on EDS measurement. As demonstrated in the EDS layered and EDS spectra in Figure 4a, five elements, including C, O, Fe, Si, and K, were detected, where the metallic elements were dominated by Fe with higher characteristic signals, and this result was consistent with the XRF analysis of the calcined solids. As shown in SEM images in Figure 4b, an increase in spherical particles was observed with a diameter of approximately 100 nm, and these particles are iron oxides. Li et al.[24] also observed nanoscale Fe_2O_3 from CRS. In addition, a lower content of the C element was detected (EDS layered and EDS spectra in Figure 4b), demonstrating that more organic matter can be removed from the solid surface during the multiple extraction processes.
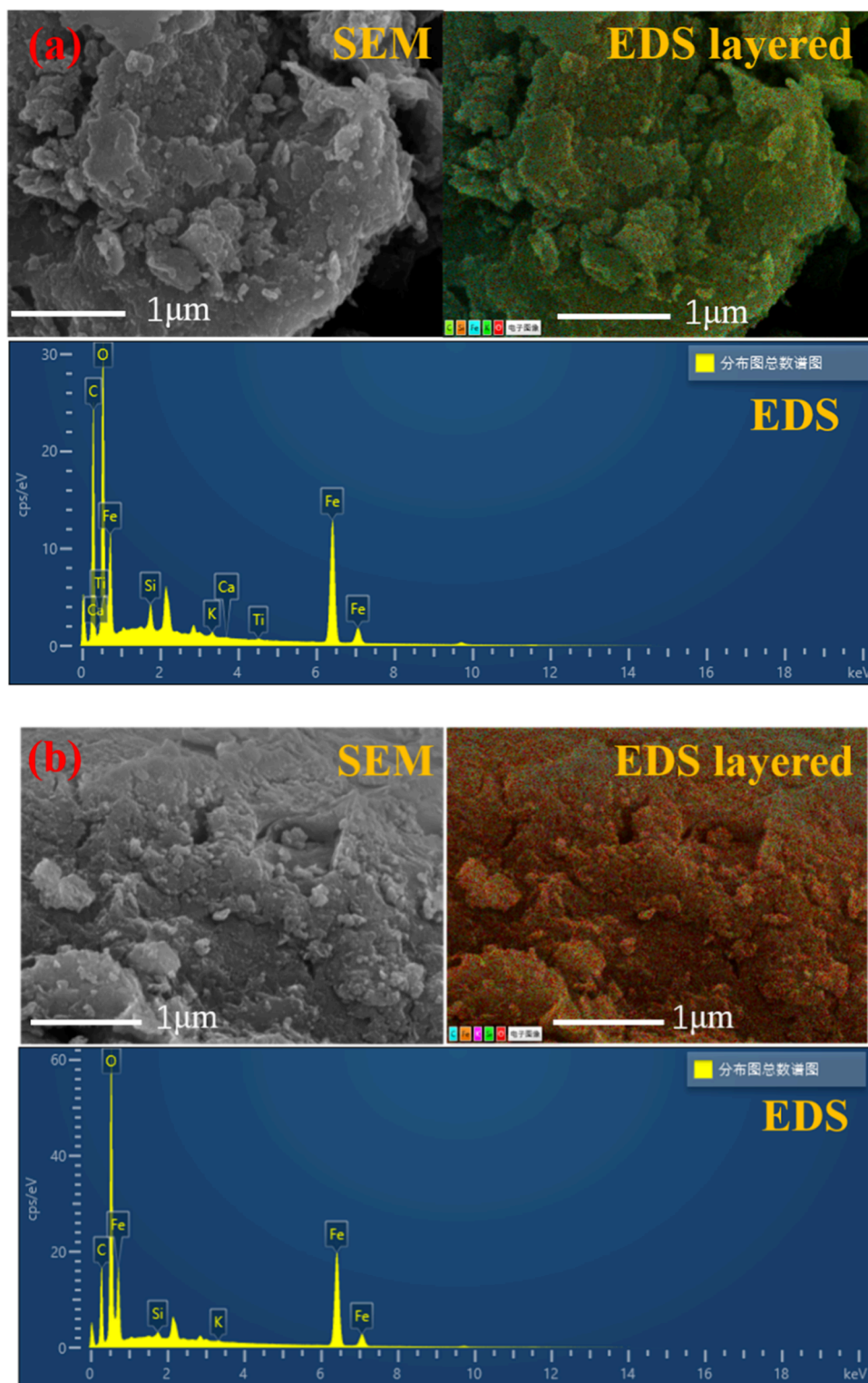
Figure 4. SEM image, EDS layered image, and EDS spectra of extracted solid: (a) single extraction; (b) third extractions.

Meanwhile, the O content measured in the EDS spectra in Figure 4b was significantly higher than that in Figure 4a. This suggested that the remaining O element is mainly derived from the solid, and it is speculated that metal iron exists in the form of Fe−O.

3.2.2. XPS analysis. The chemical states of the Fe element in the recovered solids were analyzed by XPS. As demonstrated in Figure 5, two characteristic peaks about the Fe element were detected and ascribed to Fe $2p_{1/2}$ and Fe $2p_{3/2}$, respectively.[23] Through peak splitting, two Fe^{2+} peaks at binding energies of 710.85 and 724.07 eV and two Fe^{3+} peaks at 713.25 and 725.71 eV were obtained, indicating the presence of FeO and Fe_2O_3. This result was consistent with the SEM analysis of the extracted solids. The total peak area ratio of Fe^{2+}/Fe^{3+} was semiquantitatively calculated to be 1.77, indicating that most of the iron oxides on the recovered solid surface were FeO.
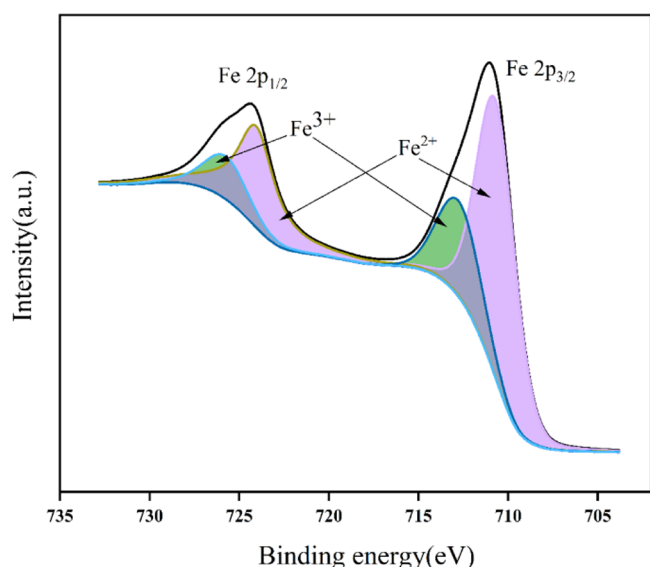
Figure 5. XPS pattern of Fe 2p in the recovered solids.

3.2.3. FT-IR Analysis. The formation mechanism of the sludge was also investigated by FT-IR analysis. The functional groups of the initially rolled sludge are shown in Figure 6a. As can be observed, an intense characteristic band at around 3455 cm^{-1} was attributed to the stretching of free O−H. Since all samples were dried before testing, it was not possible to originate from H_2O in the sludge. Meanwhile, the measurements of the saponification value and acid value indicated that palm oil (the base oil in lubricants) could generate fatty acids and hydroxylated products (monoglyceride, diglycerides, and glycerol) through hydrolysis after long-term use.[25] The peaks at 2925−2850 and 1642 cm^{-1} corresponded to the C−H and C=O groups in the fatty acids, respectively.[29] In addition, the characteristic peak at 1090 cm^{-1} was attributed to the C−C

bond on the long carbon chains.[10] The peak at 622 cm^{-1} is associated with the Fe−O bond in iron oxides, which is consistent with the above analysis of SEM and XPS.

Figure 6b reveals the FT-IR spectrum of the recovered solid after a single extraction. The same characteristic peaks as that in Figure 6a were detected and accompanied by a change in peak intensity. The intensity of the peak at 579 cm^{-1} (Fe−O bond) was significantly increased, proving that the organic matter absorbed on the solid surface was removed, and more metal oxides were exposed during the extraction. Moreover, two new characteristic peaks at 1537 and 1420 cm^{-1} appeared in Figure 6b,c, attributing to the asymmetric bending of CH_3 and the bending of the CH_2 groups.[30] The intensity difference between the Fe−O peak and other peaks from organic matter became more significant as the number of extraction rounds increased from one to three. As demonstrated in Figure 6d, no characteristic peaks from fatty acids were detected, indicating that fatty acids were preferentially removed during the extraction process. Although the peak intensity was appreciably weakened, the characteristic peak of the originating O−H group was still found at 3419 cm^{-1}. Meanwhile, characteristic peaks about CH_3 and CH_2 were detected at 1567 and 1378 cm^{-1}, respectively, suggesting the presence of hydroxylation products on the metal oxide surface that were challenging to be extracted.

Based on SEM, XPS, and FT-IR detection results, the formation mechanism of sludge is proposed in Figure 7. First, iron oxides were produced on the surface of the iron powders under high temperature and pressure during the rolling process. Due to the presence of hollow orbitals of iron atoms, the iron oxides exhibited a tetrahedral coordination iron structure (hydroxyl groups are common ligands).[31] The hydroxylated products were strongly adsorbed onto the surface of iron oxides through hydrogen bonding, forming the initial layer of adsorption. Moreover, fatty acids are present in the vicinity of the hydroxylated products due to the entanglement
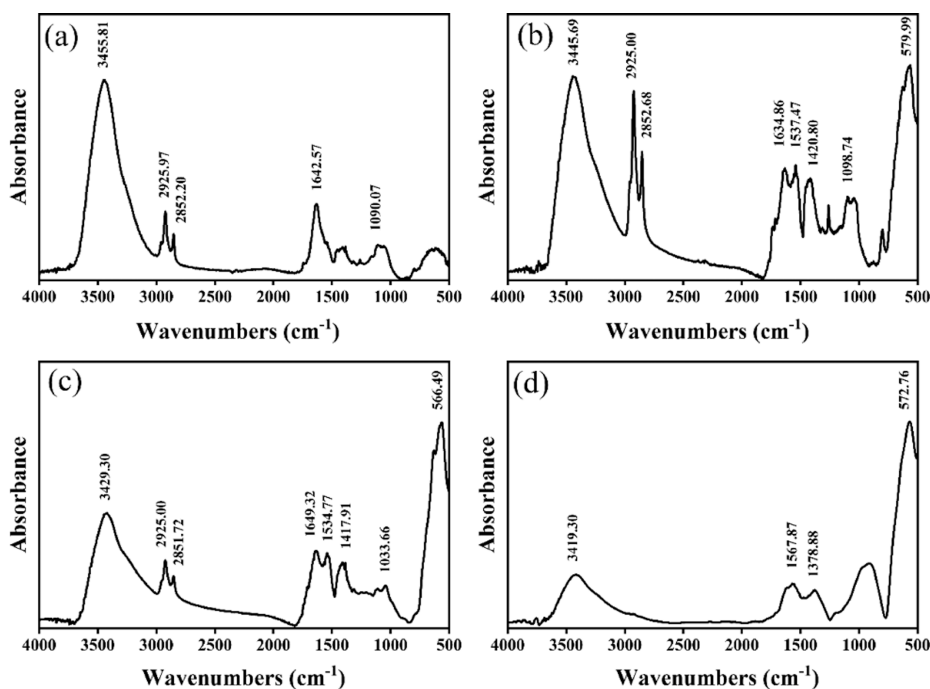
Figure 6. FT-IR spectra of (a) cold-rolled sludge, (b) single extraction, (c) twice extraction, and (d) third extraction.
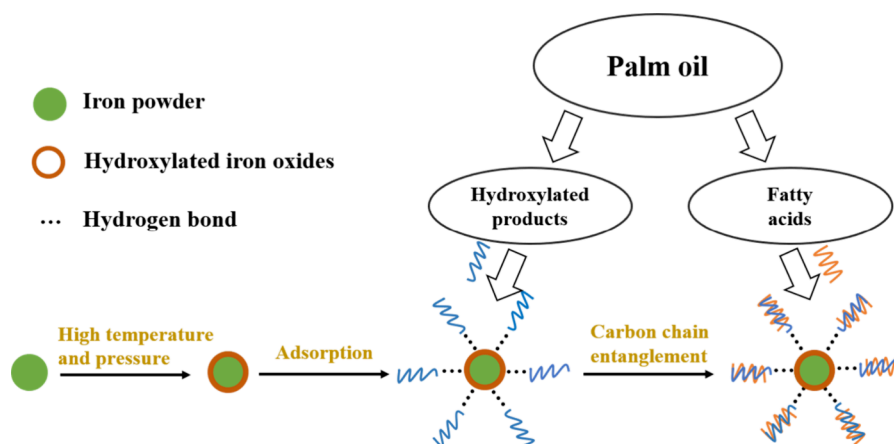
Figure 7. Formation mechanism of CRS.

of carbon chains, forming a secondary layer of adsorption. Due to the weak entanglement between the carbon chains, the fatty acids in the CRS were preferentially removed during the extraction process. The existence of hydrogen bonds makes it difficult to transfer hydroxylated products from the surface of the metal oxide to the extractant. As a result, a small amount of the organic matter remained on the extracted solid after multiple washes.

3.3. Optimization of the Extraction Condition. *3.3.1. Effect of Solvent-to-Sludge Mass Ratio.* As shown in Figure 8, the effect of the solvent-to-sludge mass ratio (4:1,
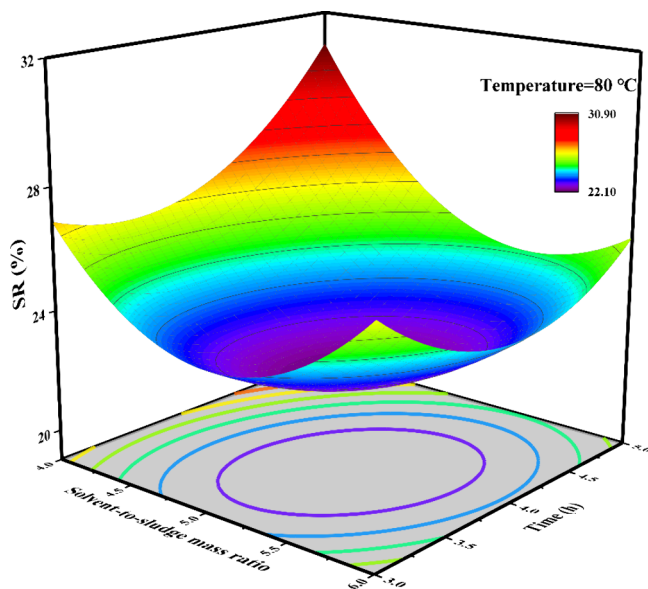
Figure 8. Three-dimensional plots of extracted solid residual oil % based on the solvent-to-sludge mass ratio and extraction time (temperature, 80 °C).

5:1, and 6:1) on the extracted solid residual oil content was investigated at a 1,2-dichloroethane/isopropyl alcohol mass ratio of 5:1. It was found that the residual oil content of the extracted solid first decreased and then increased with the increase in the solvent-to-sludge mass ratio and the lowest residual oil content was obtained at the ratio of 5.2:1. When more solvent was added, the viscosity of the system was reduced and the mass transfer between solvent and sludge would be promoted, leading to increased oil dissolved in the

solvent and decreased residual oil on the solid surface. However, an increase in residual oil content was observed when the solvent-to-oil mass ratio exceeded 5.2:1. The addition of a small amount of isopropyl alcohol was beneficial in reducing the start-up time of the extraction, promoting the entry of the oil into the organic phase at the interface and improving the extraction efficiency.[32] However, excessive isopropyl alcohol would lead to poor separation between oil and sludge, and high molecular weight oils were insoluble in the solvent with a high content of isopropyl alcohol, which was detrimental to the extraction of the oil.[27] The extraction of CRS using pure isopropyl alcohol resulted in a residual oil content of 92.1% in the extracted solids, indicating that alcohols are not ideal solvents for oil recovery from CRS. The alcohol-to-oil mass ratio needs to be controlled, and the optimal solvent-to-sludge mass ratio was 5.2:1.

3.3.2. Effect of Extraction Time. The effect of the extraction time (3, 4, and 5 h) on the extracted solid residual oil content was also explored. As shown in Figure 9, the extracted solid residual oil content kept decreasing with increasing extraction
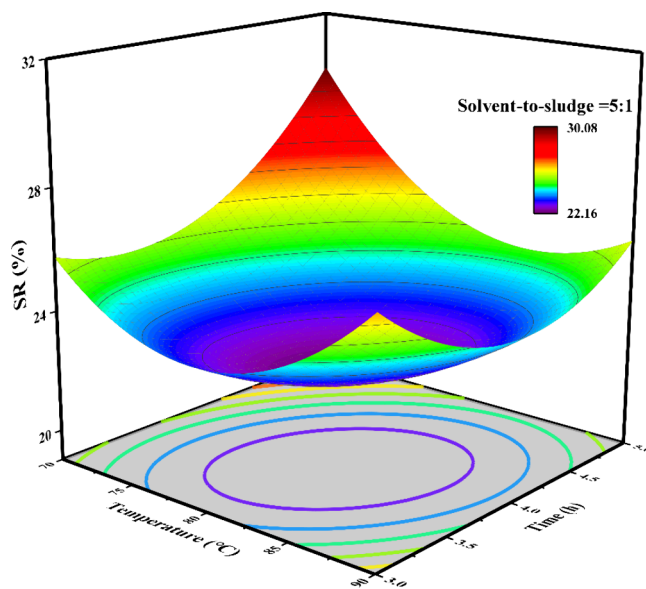
Figure 9. Three-dimensional plots of extracted solid residual oil % based on the extraction temperature and extraction time (solvent-to-sludge mass ratio, 5:1).

time when the extraction time was below 3.8 h. However, the extracted solid residual oil content did not decrease with the increase in extraction time, exceeding 3.8 h, which can be explained by the equilibrium stability and solvent saturation.[33] After 3.8 h of extraction, the equilibrium between the extraction of palm oil molecules by organic solvent and reverse extraction was achieved. Once palm oil dissolved in the solvent reached saturation, the distribution of oil molecules in the solvent would not be altered, resulting in the amount of extracted solid residual oil not being reduced with a further increase in the extraction time. Hence, the optimal extraction time was determined to be 3.8 h.

3.3.3. Effect of Extraction Temperature. The effect of the extraction temperature (70, 80, and 90 °C) on the residual oil content is shown in Figure 10. The residual oil content
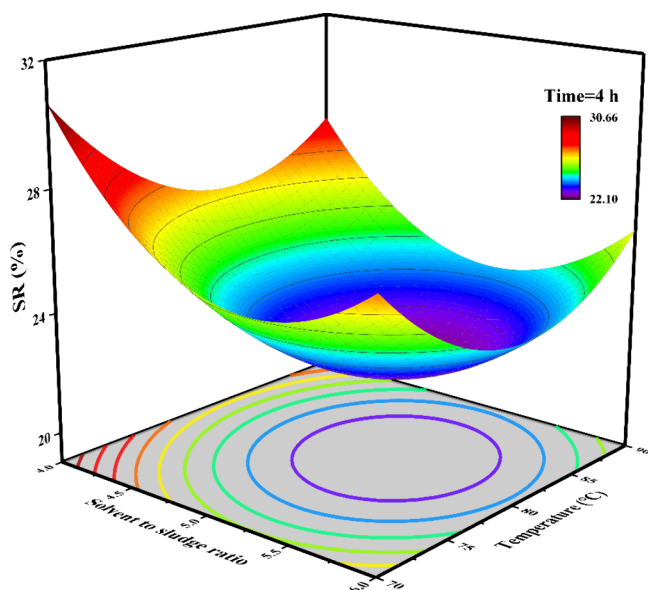
Figure 10. Three-dimensional plots of extracted solid residual oil % based on the solvent-to-sludge mass ratio and extraction temperature (time, 4 h).

decreased from 30.66 to 20.10% as the temperature increased from 70 to 81.1 °C, but no decrease in residual oil content was observed after the temperature was above 81.1 °C. High temperature expedites the transfer of organic matter from the surface of solid particles to the solvent.[33] The thermal movement between molecules became intense at higher temperatures, leading to an increase in the number of active molecules, which would facilitate forward extraction and achieve a better extraction effect. As we all know, the bubble points of 1,2-dichloroethane and isopropyl alcohol are 83.7 and 82.5 °C, respectively. When the temperature was near or above the bubble point, most of the solvents would get caught in the cycle of evaporation and condensation, which was not conducive to mass transfer between the solvent and the oil sludge, eventually leading to a decrease in the extraction efficiency. Consequently, the optimal extraction temperature for the extraction process was determined as 81.1 °C.

3.3.4. Multiple Extractions under Optimal Conditions. The optimal solvent-to-sludge mass ratio, extraction temperature, and extraction time were determined to be 5.2:1, 81.1 °C, and 3.8 h, respectively, based on the experimental results of the surface method design, and the residual oil content in the

extracted solid was reduced from 62.80 to 22.10% under the optimal condition. Furthermore, the recovered solid was repeatedly extracted three times under optimal conditions, resulting in a final solid residual oil content of approximately 10%, which was consistent with the strong hydrogen bond adsorption predicted in Section 3.2. This indicated that the hydroxylated products adsorbed on the surface through hydrogen bonding were difficult to remove by solvent extraction.

3.4. Response Analysis of Variance. The extraction conditions were optimized by Box-Behnken Design Response experiments. The solvent-to-oil mass ratio, extraction time, and extraction temperature were selected as the research objects, while the extracted solid residual oil content was set as the response factor. The experimental design and results are listed in Table 2.

The accuracy of the model was judged by the analysis of variance (ANOVA), with a *P*-value of 0.05 being used as the threshold for statistical significance and identification of significance.[34] The coefficient of variance (R^2) and adjusted coefficient of variance (R_{adj}^2) were other important criteria.[35] The crucial statistics associated with the model are reported in Table 6. It was found that the *P*-value of the model in this

Table 6. Analysis of Variance for the Solid Phase Residual Oil Model

factor	SS	df	MS	*F*-value	*P*-value
model	138.67	9	15.41	100.56	<0.0001
X_1	14.31	1	14.31	93.41	<0.0001
X_2	5.28	1	5.28	34.47	0.0006
X_3	6.48	1	6.48	42.29	0.0003
$X_1 \cdot X_2$	0.56	1	0.56	3.67	0.0969
$X_1 \cdot X_3$	4.84	1	4.84	31.59	0.0008
$X_2 \cdot X_3$	6.25	1	6.25	40.79	0.0004
X_1^2	41.45	1	41.45	270.52	<0.0001
X_2^2	30.41	1	30.41	198.49	<0.0001
X_3^2	18.79	1	18.79	122.64	<0.0001
residual	1.07	7	0.15		
lack of fit	0.79	3	0.26	3.77	0.1161
pure error	0.28	4	0.070		
cor total	139.74	16			

study was below 0.0001, indicating that the model was significant and the differences between the model and experimental results were caused by a random error with a probability of less than 1%. Moreover, the *P*-values of X_1, X_2, and X_3 were all less than 0.05, suggesting that all three had a significant effect on the response values. The maximum *F* values obtained from the ANOVA results show that the solvent-to-sludge mass ratio (X_1) had been the best significant parameter that influenced SR%. Meanwhile, the *P*-value lacking fit was 0.1161 (>0.05 was not significant), which meant that the model fitted well with the experimental data.

The comparison of the predicted values of the second-order model with the observed values of SR% is shown in Figure 11. In the solid phase residual oil model, R^2 and R_{adj}^2 were determined to be 0.9923 and 0.9825, respectively, proving that the model was trustworthy.

The quadratic regression equation was obtained using the least-squares error method, and the extracted solid residual oil content after multiple iterations is presented in eq 6:
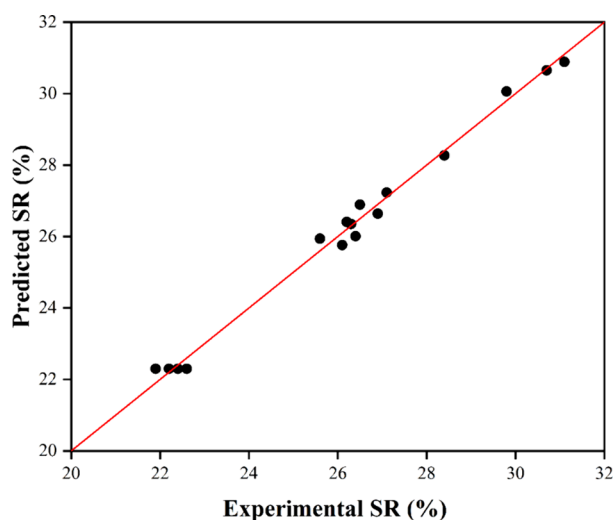
Figure 11. Comparing the experimental and predicted values of SR (%).

$$SR\% = 269.125 - 31.313X_1 - 4.069X_2 - 0.500X_3$$
$$+ 0.038X_1 \cdot X_2 - 1.100X_1 \cdot X_3 - 0.125X_2 \cdot X_3$$
$$+ 3.138X_1^2 + 0.027X_2^2 + 2.112X_3^2 \quad (6)$$

where X_1, X_2, and X_3 are the solvent-to-sludge mass ratio, extraction temperature, and extraction time, respectively. Based on the equation obtained, the relationship between the variables and the yield of recovered oil can be further investigated.

3.5. Analysis of Factors Influencing Biodiesel Preparation. *3.5.1. Effect of H_2SO_4 Dosage on Biodiesel Yield.* As displayed in Figure 12, the effect of H_2SO_4 dosage (15−35 wt
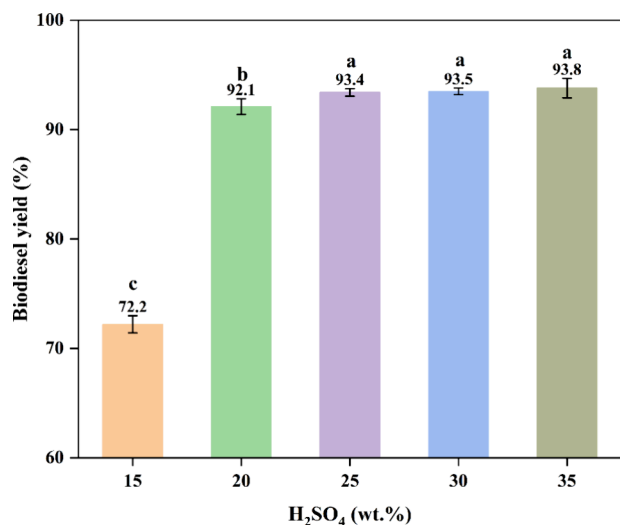
Figure 12. Effect of the H_2SO_4 dosage on biodiesel yield.

%) on the yield of biodiesel was first explored when the reaction time was 16 h, the methanol-to-oil molar ratio was 70:1, and the reaction temperature was 70 °C. It was found that the yield of biodiesel was proportional to the dosage of sulfuric acid.[36] The yield of biodiesel produced from the extracted oil was less than 75% at a catalyst concentration of 15 wt %, whereas it was more than 92% when the H_2SO_4 dosage

was 20 wt %. A tiny increase in the yield was detected at a catalyst dosage above 25 wt % accompanied by the first disappearance of the acidic gums as byproducts. Increased catalyst dosage helps to curb acidic gum production. The study indicated that H_2SO_4, a Brønsted acid, is more active in the esterification reaction than in the transesterification reaction.[37] Considering that the esterification reaction and ester exchange reaction are carried out simultaneously, to ensure the activity of the catalyst and reduce the production of byproduct acidic gum during the ester exchange process, 25 wt % was chosen as the optimum catalyst dosage.

3.5.2. Effect of Reaction Time on Biodiesel Yield. Figure 13 reveals the effect of reaction time (8−28 h) on biodiesel yield
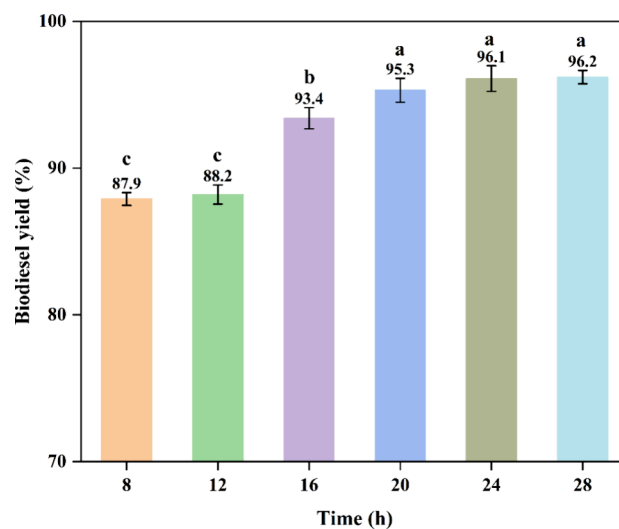
Figure 13. Effect of reaction time on biodiesel yield.

when the H_2SO_4 dosage, methanol-to-oil molar ratio, and reaction temperature were 25 wt %, 70:1, and 70 °C, respectively. By increasing the reaction time, the reaction moved in the forward reaction, which ultimately augmented the biodiesel production. The highest biodiesel yield of 96.2% was obtained at the reaction time of 28 h, but the increasing reaction time exceeding 20 h did not result in a significant increase in biodiesel yield. In the static separation, three phases were observed, with the middle phase being a viscous flocculent acidic gum. After the reaction reached 24 h, no viscous acidic colloid was observed after distillation to recover methanol, and the subsequent static separation was in two phases, so prolonging time is conducive to reduced acidic gum production. Meanwhile, considering the composition of extracted oil, the esterification reaction and transesterification reaction coexist in the experiment. The esterification reaction rate is slower than the transesterification reaction,[38] so prolonging time is conducive to the positive progress of the transesterification reaction. Nevertheless, when the dynamic equilibrium was formed after 24 h of reaction, prolonging the reaction time could not effectively improve the yield but rather increased energy consumption. Therefore, the optimal reaction time was determined to be 24 h.

3.5.3. Effect of Methanol-to-Oil Molar Ratio on Biodiesel Yield. The effect of the molar ratio of methanol to oil (50:1−110:1) on biodiesel yield was studied when H_2SO_4 dosage was 25 wt %, reaction time was 24 h, and reaction temperature was 70 °C. As shown in Figure 14, the yield of biodiesel rose as the
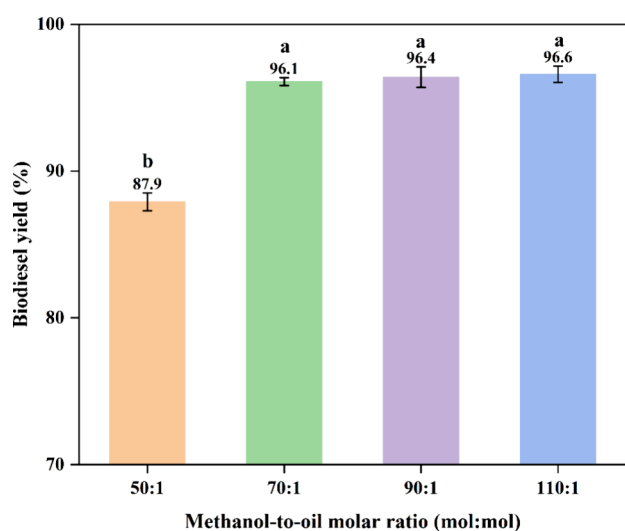
Figure 14. Effect of the methanol-to-oil molar ratio on biodiesel yield.

Figure 15. Effect of the reaction temperature on biodiesel yield.

methanol-to-oil molar ratio increased. As can be seen from Figure 14, the highest yield of biodiesel of 96.6% was obtained at a molar ratio of 110:1. In addition, there was no significant increase in the biodiesel yield, as the molar ratio of methanol-to-oil exceeded 70:1. Theoretically, acid-catalyzed trans-esterification is a reversible reaction requiring three moles of alcohol for the esterification of 1 mole of triglyceride.[39] The addition of excess methanol in the actual reaction further increased the yield by reducing the viscosity of the oil while increasing the mass and heat transfer, and more reagents would be wasted.[40] When the said molar ratio increased from 70:1 to 110:1, the increase in biodiesel yield was negligible (0.05%), which is due to the fact that the increased amount of methanol would lead the hydroxyl group to emulsification,[41] exacerbating the difficulty of product separation and ultimately leading to a slow increase in biodiesel yield. Meanwhile, the increase in methanol consumption resulted in an increase in operating costs and energy consumption for the removal of abundant methanol. Thus, the molar ratio of methanol to oil should be maintained at 70:1.

3.5.4. Effect of Reaction Temperature on Biodiesel Yield. The reaction temperature is a pivotal parameter that affects the rate of reaction. The effect of reaction temperature (50–90 °C) on biodiesel yield when H_2SO_4 dosage is 25 wt %, reaction time is 24 h, and the methanol-to-oil molar ratio is 70:1 is depicted in Figure 15. As can be seen, the yield of biodiesel first increased and then decreased as the temperature raised from 50 to 90 °C. The highest biodiesel yield of 96.5% was obtained at 60 °C. A higher temperature is favorable to the increase in active molecule concentration and the promotion of intermolecular collisions, ultimately leading to an increase in the reaction rate.[42] However, when the temperature exceeded 60 °C, the viscosity of the system would increase due to the boiling loss of methanol, which further led to the decline of the biodiesel yield. Furthermore, a previous study[43] concluded that the polymerization between unsaturated fatty acids and esters would be promoted when the temperature was above 60 °C, which was also detrimental to biodiesel yield. Therefore, the optimum reaction temperature for the production of biodiesel was 60 °C.

3.5.5. Properties of Biodiesel Products. The ASTM standard was chosen to evaluate the main quality of the
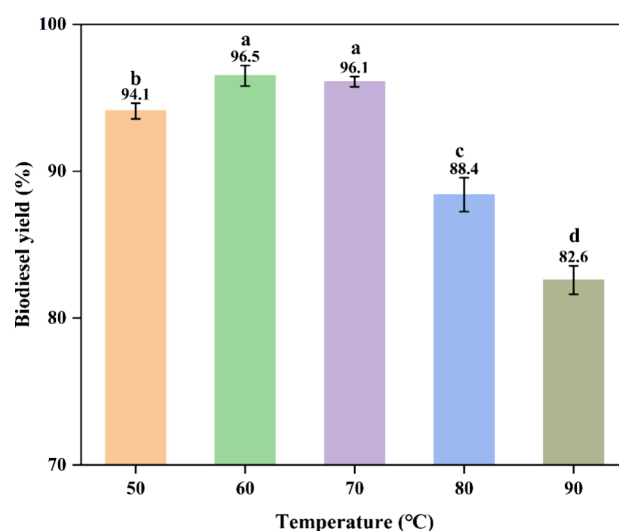
biodiesel.[44] The results given in Table 7 show that its kinematic viscosity, acid number, total glycerin, moisture

Table 7. Main Properties of Biodiesel Products against ASTM D6751/EN 14214

property	test method	value	ASTM D6751/ EN 14214
density (kg/m³, 15 °C)	EN ISO 3675	875.3	860–900 (EN 14214)
kinematic viscosity (mm²/ s, 40 °C)	ASTM D445	5.34	1.9–6.0
acid number (mg KOH/g)	ASTM D664	0.37	0.50 max
total glycerin (wt %)	ASTM D6584	0.18	0.240 max
moisture content (mg/kg)	ASTM D2709	247	500 max
FAME content (wt %)	EN 14103	98.79	96.5 min (EN 14214)
flashpoint (°C)	ASTM D93	147	130 min
cetane number	ASTM D613	54	47 min

content, flashpoint, and cetane number all meet the requirements of the ASTM D6751 standard, indicating the high quality of the biodiesel products. It is worth noting to say that as the ASTM standard has not provided a range for the density and FAME content, we compared them to the EN 14214 standard. The values in the table are average values after repeating the process three times. The data presented have a standard deviation (SD) of less than 2%.

4. CONCLUSIONS

In this article, the formation mechanism of CRS was verified by its comprehensive analysis through SEM-EDS, XPS, and FT-IR. The oil in CRS was extracted by a mixture of 1,2-dichloroethane and isopropanol. H_2SO_4 was employed as a homogeneous catalyst, simultaneously catalyzing the extracted oil from CRS and methanol for esterification and trans-esterification. The optimum biodiesel yield of 96.5% was achieved when the H_2SO_4 dosage was 25 wt %, the reaction time was 24 h, the methanol-to-oil molar ratio was 70:1, and the reaction temperature was 60 °C. Finally, the main properties of biodiesel products were verified to meet the ATSM D6751 standard. This paper provides new ideas and

requisite data for the resource utilization of CRS to give value-added products.

AUTHOR INFORMATION

Corresponding Author

　　Xiaolong Zhou − *International Joint Research Center of Green Chemical Engineering, School of Chemical Engineering, East China University of Science and Technology, Shanghai 200237, China*; Email: xiaolong@ecust.edu.cn

Authors

　　Mengke Zhou − *International Joint Research Center of Green Chemical Engineering, School of Chemical Engineering, East China University of Science and Technology, Shanghai 200237, China*; ⊙ orcid.org/0009-0000-0997-8169

　　Peng Jiang − *International Joint Research Center of Green Chemical Engineering, School of Chemical Engineering, East China University of Science and Technology, Shanghai 200237, China*; ⊙ orcid.org/0000-0003-3743-6177

　　Yichao Hu − *International Joint Research Center of Green Chemical Engineering, School of Chemical Engineering, East China University of Science and Technology, Shanghai 200237, China*

　　Muhammad-Faryad Ali − *International Joint Research Center of Green Chemical Engineering, School of Chemical Engineering, East China University of Science and Technology, Shanghai 200237, China*

Complete contact information is available at:
https://pubs.acs.org/10.1021/acsomega.3c02027

Notes

The authors declare no competing financial interest.

REFERENCES

(1) Ye, H.; Li, Q.; Yu, H.; Xiang, L.; Wei, J.; Lin, F. Pyrolysis behaviors and residue properties of iron-rich rolling sludge from steel smelting. *Int. J. Environ. Res. Public Health* **2022**, *19*, 2152.

(2) Hamann, C.; Spanka, M.; Stolle, D.; Auer, G.; Weingart, E.; Al-Sabbagh, D.; Ostermann, M.; Adam, C. Recycling of blast-furnace sludge by thermochemical treatment with spent iron (II) chloride solution from steel pickling. *J. Hazard. Mater.* **2021**, *402*, No. 123511.

(3) Lin, F.; Xiang, L.; Sun, B.; Li, J.; Yan, B.; He, X.; Liu, G.; Chen, G. Migration of chlorinated compounds on products quality and dioxins releasing during pyrolysis of oily sludge with high chlorine content. *Fuel* **2021**, *306*, No. 121744.

(4) Zulqarnain; Ayoub, M.; Yusoff, M. H. M.; Nazir, M. H.; Zahid, I.; Ameen, M.; Sher, F.; Floresyona, D.; Budi Nursanto, E. A comprehensive review on oil extraction and biodiesel production technologies. *Sustainability* **2021**, *13*, 788.

(5) Kim, J. H.; Oh, J. I.; Baek, K.; Park, Y. K.; Zhang, M.; Lee, J.; Kwon, E. E. Thermolysis of crude oil sludge using CO_2 as reactive gas medium. *Energy Convers. Manage.* **2019**, *186*, 393−400.

(6) Gao, N.; Jia, X.; Gao, G.; Ma, Z.; Quan, C.; Naqvi, S. R. Modeling and simulation of coupled pyrolysis and gasification of oily sludge in a rotary kiln. *Fuel* **2020**, *279*, No. 118152.

(7) Lin, Z.; Xu, F.; Wang, L.; Hu, L.; Zhu, L.; Tan, J.; Li, Z.; Zhang, T. Characterization of oil component and solid particle of oily sludge treated by surfactant-assisted ultrasonication. *Chin. J. Chem. Eng.* **2021**, *34*, 53−60.

(8) Chen, W. S.; Chen, Y. C.; Lee, C. H. Hydrometallurgical Recovery of Iron, Nickel, and Chromium from Stainless Steel Sludge with Emphasis on Solvent Extraction and Chemical Precipitation. *Processes* **2022**, *10*, 748−759.

(9) Yaseen, M.; Ullah, M.; Subhan, S.; Ahmad, W.; Subhan, F.; Shakir, M. Recovery and characterization of useful benzene derivatives from spent engine oil through solvent extraction. *Chem. Eng. Res. Des.* **2021**, *175*, 51−60.

(10) Zhao, J.; Yuan, C.; Yao, X. A simple method to evaluate solvent for lubricating oil by solubility parameter. *Pet. Sci. Technol.* **2017**, *35*, 1445−1450.

(11) Gouran, A.; Aghel, B.; Nasirmanesh, F. Biodiesel production from waste cooking oil using wheat bran ash as a sustainable biomass. *Fuel* **2021**, *295*, No. 120542.

(12) Pikula, K.; Zakharenko, A.; Stratidakis, A.; Razgonova, M.; Nosyrev, A.; Mezhuev, Y.; Tsatsakis, A.; Golokhvast, K. The advances and limitations in biodiesel production: feedstocks, oil extraction methods, production, and environmental life cycle assessment. *Green Chem. Lett. Rev.* **2020**, *13*, 275−294.

(13) dos Santos, R. C. M.; Gurgel, P. C.; Pereira, N. S.; Breves, R. A.; de Matos, P. R. R.; Silva, L. P.; Sales, M. J. A.; Lopes, R. d. V. V. Ethyl esters obtained from pequi and macaúba oils by transesterification with homogeneous acid catalysis. *Fuel* **2020**, *259*, No. 116206.

(14) Maquirriain, M. A.; Querini, C. A.; Pisarello, M. L. Glycerine esterification with free fatty acids: Homogeneous catalysis. *Chem. Eng. Res. Des.* **2021**, *171*, 86−99.

(15) Bashir, M. A.; Wu, S.; Zhu, J.; Krosuri, A.; Khan, M. U.; Ndeddy Aka, R. J. Recent development of advanced processing technologies for biodiesel production: A critical review. *Fuel Process. Technol.* **2022**, *227*, No. 107120.

(16) Kunh, S. S.; Kugelmeier, C. L.; Mantovan, F. d. M.; Lenz, G. F.; Sattolo, N. M. S.; Milinsk, M. C.; Alves, H. J. Valorization of poultry slaughterhouse sludge oil: a strategy to reduce Brazil's dependency on soybean oil in the biodiesel industry. *Environ. Technol.* **2022**, *43*, 2177−2189.

(17) ASTM, D. 95, Standard Test Method for Water in Petroleum Products and Bituminous Materials by Distillation. *Annual Book of Standards* **2018**.

(18) Standard, A. S. T. M. Standard Test Method for Acid and Base Number by Color-Indicator Titration. *Annual Book of Standards* 2021.

(19) ASTM, D. Standard Test Method for Specific Gravity, Apparent, of Liquid Industrial Chemicals. *Annu. Book ASTM Stand*, 2018, 15.

(20) Zhang, Y.; Niu, S.; Lu, C.; Gong, Z.; Hu, X. Catalytic performance of $NaAlO_2/\gamma$-Al_2O_3 as heterogeneous nanocatalyst for biodiesel production: Optimization using response surface methodology. *Energy Convers. Manage.* **2020**, *203*, No. 112263.

(21) Chen, G.; Li, J.; Li, K.; Lin, F.; Tian, W.; Che, L.; Yan, B.; Ma, W.; Song, Y. Nitrogen, sulfur, chlorine containing pollutants releasing characteristics during pyrolysis and combustion of oily sludge. *Fuel* **2020**, *273*, No. 117772.

(22) Gao, J.; Lu, C.; Su, W.; Li, Z.; Li, X.; Zhao, Y.; Deng, G.; Li, K. Exploring the effect of calcination temperature and sulphuric acid impregnation treatment on the NH3-SCR activity of cold-rolled sludge. *Process Saf. Environ. Prot.* **2022**, *161*, 658−668.

(23) Li, Y.; Cheng, H.; Li, G.; Mei, X.; Lu, X.; Xu, Q. Experimental Study on Dechlorination of Cold-Rolling Sludge at High-Temperature Roasting. In *10th International Symposium on High-Temperature Metallurgical Processing*; Springer International Publishing: 2019; pp 657−663.

(24) Zhu, S.; Li, T.; Wu, Y.; Chen, Y.; Su, T.; Ri, K.; Huo, Y. Effective purification of cold-rolling sludge as iron concentrate powder via a coupled hydrothermal and calcination route: From laboratory-scale to pilot-scale. *J. Cleaner Prod.* **2020**, *276*, No. 124274.

(25) Chen, L.; He, L.; Zheng, B.; Wei, G.; Li, H.; Zhang, H.; Yang, S. Bifunctional acid-activated montmorillonite catalyzed biodiesel production from non-food oil: Characterization, optimization, kinetic and thermodynamic studies. *Fuel Process. Technol.* **2023**, *250*, No. 107903.

(26) Abdel Aziz, M. S.; Salama, H. E. Development of alginate-based edible coatings of optimized UV-barrier properties by response

surface methodology for food packaging applications. *Int. J. Biol. Macromol.* **2022**, *212*, 294−302.

(27) Zgheib, N.; Takache, H. Recycling of used lubricating oil by solvent extraction: experimental results, Aspen Plus simulation and feasibility study. *Clean Technol. Environ. Policy* **2021**, *23*, 65−76.

(28) Valladares-Diestra, K.; de Souza Vandenberghe, L. P.; Soccol, C. R. Oilseed Enzymatic Pretreatment for Efficient Oil Recovery in Biodiesel Production Industry: a Review. *BioEnergy Res.* **2020**, *13*, 1016−1030.

(29) Bashir, M. A.; Wu, S.; Krosuri, A. Rapid and efficient esterification of oleic acid by continuous liquid-phase plasma discharge. *J. Environ. Chem. Eng.* **2021**, *9*, No. 104640.

(30) Meng, F.; Ma, S.; Muhammad, Y.; Li, J.; Sahibzada, M.; Chi, F. Analysis of virgin asphalt brands via the integrated application of FT-IR and gel permeation chromatography. *Arabian J. Sci. Eng.* **2020**, *45*, 7999−8009.

(31) Qu, Z.; Wu, Y.; Zhu, S.; Yu, Y.; Huo, M.; Zhang, L.; Yang, J.; Bian, D.; Wang, Y. Green synthesis of magnetic adsorbent using groundwater treatment sludge for tetracycline adsorption. *Engineering* **2019**, *5*, 880−887.

(32) Shen, Y.; Zhang, Q.; Sun, X.; Zhang, Y.; Cai, Q.; Deng, W.; Rao, S.; Wu, X.; Ye, Q. Conversion of wet microalgae to biodiesel with microalgae carbon based magnetic solid acid catalyst. *Energy Convers. Manage.* **2023**, *286*, No. 117022.

(33) Comerlatto, A.; Voll, F. A.; Daga, A. L.; Fontana, É. Mass transfer in soybean oil extraction using ethanol/isopropyl alcohol mixtures. *Int. J. Heat Mass Transfer* **2021**, *165*, No. 120630.

(34) You, Y.; Liu, C.; Xu, Q.; Hu, X.; Zhang, S.; Wang, C.; Guo, H.; Tang, C. Response surface methodology to optimize ultrasonic-assisted extraction of crude oil from oily sludge. *Pet. Sci. Technol.* **2022**, *40*, 2082.

(35) Chen, X.; Zhang, Y.; Xu, B.; Li, Y. A simple model for estimation of higher heating value of oily sludge. *Energy* **2022**, *239*, No. 121921.

(36) Ning, Y.; Niu, S.; Wang, Y.; Zhao, J.; Lu, C. Sono-modified halloysite nanotube with $NaAlO_2$ as novel heterogeneous catalyst for biodiesel production: optimization via GA-BP neural network. *Renewable Energy* **2021**, *175*, 391−404.

(37) Munyentwali, A.; Li, H.; Yang, Q. Review of advances in bifunctional solid acid/base catalysts for sustainable biodiesel production. *Appl. Catal., A* **2022**, *633*, No. 118525.

(38) Pan, H.; Xia, Q.; Li, H.; Wang, Y.; Shen, Z.; Wang, Y.; Li, L.; Li, X.; Xu, H.; Zhou, Z.; Yang, S. Direct production of biodiesel from crude Euphorbia lathyris L. Oil catalyzed by multifunctional mesoporous composite materials. *Fuel* **2022**, *309*, No. 122172.

(39) Wancura, J. H. C.; Brondani, M.; dos Santos, M. S. N.; Oro, C. E. D.; Wancura, G. C.; Tres, M. V.; Oliveira, J. V. Demystifying the enzymatic biodiesel: How lipases are contributing to its technological advances. *Renewable Energy* **2023**, *216*, No. 119085.

(40) Rocha, P. D.; Oliveira, L. S.; Franca, A. S. Sulfonated activated carbon from corn cobs as heterogeneous catalysts for biodiesel production using microwave-assisted transesterification. *Renewable Energy* **2019**, *143*, 1710−1716.

(41) Zulqarnain; Yusoff, M. H. M.; Ayoub, M.; Nazir, M. H.; Sher, F.; Zahid, I.; Ameen, M. Solvent extraction and performance analysis of residual palm oil for biodiesel production: Experimental and simulation study. *J. Environ. Chem. Eng.* **2021**, *9*, No. 105519.

(42) Manimaran, R.; Mohanraj, T.; Prabakaran, S. Biodegradable waste-derived biodiesel as a potential green fuel: Optimization of production process and its application in diesel engine. *Ind. Crops Prod.* **2023**, *192*, No. 116078.

(43) De, A.; Boxi, S. S. Application of Cu impregnated TiO_2 as a heterogeneous nanocatalyst for the production of biodiesel from palm oil. *Fuel* **2020**, *265*, No. 117019.

(44) Cai, D.; Xie, Y.; Li, L.; Ren, J.; Lin, X.; Qiu, T. Design and synthesis of novel Brønsted-Lewis acidic ionic liquid and its application in biodiesel production from soapberry oil. *Energy Convers. Manage.* **2018**, *166*, 318−327.